Solvent and compartmentalization effects on the photophysics of 4-(benzothiazol-2-yl)-N,N-diphenylaniline

Silvana Valdebenito, Renzo Zanocco, Germán Günther, Else Lemp and Antonio L. Zanocco*

[1]Universidad de Chile, Facultad de Ciencias Químicas y Farmacéuticas, Departamento de Química Orgánica y Fisicoquímica, Casilla 233, Santiago - 1, Santiago, Chile,

Efectos de disolvente y la compartimentalización en la fotofísica de 4 - (benzotiazol-2-il)-N, N-diphenylaniline
Efectes de dissolvent i la compartimentació fotofísica de 4 - (benzotiazol-2-il)-N, N-diphenylaniline
Recibido: 20 de mayo de 2011; aceptado: 26 de mayo de 2011

RESUMEN

Se estudiaron las propiedades fotofísicas del 4-(benzotiazol-2-il)-N,N-difenilamilina en una serie de solventes. Los espectros de absorción UV-Vis, son independientes de la polaridad del solvente, mientras que los espectros de fluorescencia obtenidos en el mismo conjunto de solventes muestran un importante efecto solvatocrómico que produce grandes corrimientos de Stokes. Se emplearon relaciones lineales de energía libre de solvatación para correlacionar la posición del máximo del espectro de fluorescencia con parámetros empíricos microscópicos del solvente. Este estudio, indica que durante el proceso de excitación, se produce una significativa transferencia intramolecular de carga. Además, un análisis del comportamiento solvatocrómico de los espectros de fluorescencia y de absorción UV-Vis en términos de la ecuación de Lippert-Mataga, muestra un gran aumento del momento dipolar en el estado excitado, el que es también compatible con un estado excitado con transferencia intramolecular de carga. Considerando estas propiedades, nosotros exploramos el potencial uso de esta prueba fluorescente en la determinación de parámetros termodinámicos de sistemas micelares. Nosotros encontramos que el 4-(benzotiazol-2-il)-N,N-difenilanilina, puede ser ventajosamente empleado para determinar valores de la CMC de surfactantes iónicos (dodecil sulfato de sodio) y no iónicos (Tritón X-100 y monocaprato de sacarosa) y las constantes de reparto de n-alcoholes en micelas de SDS.
Palabras clave: Fotofísica; benzotiazoles; transferencia intramolecular de carga; micelas; CMC; constante de reparto**.**

SUMMARY

The photophysical properties of 4-(benzothiazol-2-yl)-N,N-diphenylaniline, were studied in a series of solvents. UV–Vis absorption spectra are insensitive to solvent polarity whereas the fluorescence spectra in the same solvent set show an important solvatochromic effect leading to large Stokes shifts. Linear solvation energy relationships were employed to correlate the position of fluorescence spectra maxima with microscopic empirical solvent parameters. This study indicates that important intramolecular charge transfer takes place during the excitation process. In addition, an analysis of the solvatochromic behavior of the UV–Vis absorption and fluorescence spectra in terms of the Lippert-Mataga equation, shows a large increase of the excited-state dipole moment, which is also compatible with the formation of an intramolecular charge-transfer excited state. Given the above properties, we explored the potential of this fluorescent probe for the determination of thermodynamic parameters of micellar systems. We found that 4-(benzothiazol-2-yl)-N,N-diphenylaniline can be advantageously employed to determine CMC values of ionic (sodium dodecyl sufate) and non-ionic (Triton X-100 and sucrose monocaprate) surfactants and the partition constant of n-alcanols in SDS micelles.
Keywords: Photophysics; benzothiazoles; intramolecular charge transfer; micelles; CMC; partition constant.

RESUM

Es van estudiar les propietats fotofísiques del 4 - (benzotiazol-2-il)-N, N- difenilanilina en una sèrie de solvents. Els espectres d'absorció UV-Vis, són independents de la polaritat del solvent, mentre que els espectres de fluorescència obtinguts en el mateix conjunt de solvents mostren un important efecte solvatocròmic que produeix grans desplaçaments de Stokes. Es van emprar relacions lineals d'energia lliure de solvatació per correlacionar la posició del màxim de l'espectre de fluorescència amb paràmetres empírics microscòpics del solvent. Aquest estudi, indica que durant el procés d'excitació, es produeix una significativa transferència intramolecular de càrrega. A més a més, una anàlisi del comportament solvatocròmic dels espectres de fluorescència i d'absorció UV-Vis en termes de l'equació de Lippert-Mataga, mostra un gran augment del moment dipolar en l'estat excitat, el que és també compatible amb un estat excitat amb transferència intramolecular de càrrega. Considerant aquestes propietats, es va explorar el possible ús d'aquesta prova fluorescent en la determinació de paràmetres termodinàmics de sistemes micel·lars Es va trobar que el 4-(benzotiazol-2-il)-N,N- difenilanilina, pot ser emprat avantatjosament per determinar valors de la CMC de surfactants iònics (dodecil sulfat de sodi) i no iònics (Tritó X-100 i monocaprat de sacarosa) i les constants de repartiment de n-alcohols en micel.les de SDS.
Paraules clau: Fotofísica; benzotiazol, transferència intramolecular de càrrega; micel.la, CMC, constant de repartiment.

*Corresponding author: azanocco@ciq.uchile.cl
Phone: 56-2-9782878, Fax: 56 - 2 - 9782868.

INTRODUCTION

Exploring new fluorescent dyes and expanding the tool box of the currently available fluorescent probes for the monitoring of chemical and biological systems and processes is a challenge crucial to several research areas. The small benzothiazole nucleus has been incorporated into a wide variety of fluorescent probes. Accordingly, studies on the absorptive and emissive characteristics of benzothiazole derivatives with the aim of accounting for their applications are currently carried out. This family of compounds is endowed with large absorption coefficients in the ultraviolet, fluorescence quantum yields close to unity in a large variety of solvents, and high photostability [1,2]. These properties make benzothiazoles excellent fluorophores for a large variety of applications. Over the last few years, benzothiazoles have been studied mainly for two-photon spectroscopy developments [3,4], as amyloid fluorescent markers [5], for the quantification of metal ions [6-8], DNA detection [9,10], development of 'click-on' fluorogenic dyes [11] and in the study and determination of properties of micro-compartmentalized systems [12-14]. Recently, Wang et al., as part of a work on the synthesis and characterization of a series of dipolar compounds containing donor and acceptor materials of triphenylamine-benzothiazole [15], showed that 4-(benzothiazol-2-yl)-N,N-diphenylaniline (Figure 1) has a high extinction coefficient and fluoresces efficiently in chloroform (Φ_F = 0.66). However, this fluorescent probe neither has been fully characterized nor studies on its applications have been reported. In connection with our studies on the solvent effect on photophysics of naphthoxazole derivatives, we synthesized several benzothiazoles, including 4-(benzothiazol-2-yl)-N,N-diphenylaniline, *DPAPBTZ*. We report in this work the results of the study of effect of solvent and compartmentalization on the steady-state fluorescence of *DPAPBTZ*. The results suggest that it is a valuable fluorescent probe to determine thermodynamic parameters of micellar systems such as critical micellar concentration and partition constant of added compounds.

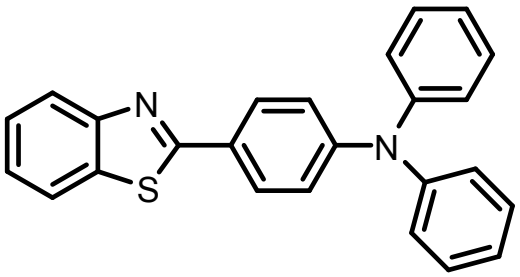

4-(benzothiazol-2-yl)-N,N-diphenylaniline

Figure.1 *Molecular estructure of DPAPBTZ*

EXPERIMENTAL DETAILS

General

All solvents used in the syntheses, spectroscopic and kinetic measurements were of reagent grade, spectroscopic or HPLC quality. NMR spectra were recorded in a Bruker Advance 300 MHz spectrometer. Chemical shifts are referred to the internal standard tetramethylsilane, TMS. Steady state fluorescence spectra were recorded in a ISS PC1 spectrofluorometer and the UV-Vis spectra in a Unicam UV-4 spectrophotometer.

Chemical Synthesis

4-(benzo[d]thiazol-2-yl)-N,N-diphenylaniline was synthesized employing a modification of a method previously described in the literature [16]. Briefly, in a porcelain mortar a mixture of 2-aminothiophenol (1 mmol), 4-diphenylaminobenzaldehyde (1 mmol) and a catalytic quantity of sublimed molecular iodine (0.5 mmol) was carefully blended at room temperature for 15 min. The reaction completion was verified using thin-layer chromatography. Then, the mixture was dissolved in small volume of methylene dichloride and chromatographed over silica gel using petroleum ether-ethyl acetate (4:1) to afford the pure product. Yield 96%, m.p. = 146-149 °C, ^{1}H-NMR($CDCl_3$) δ: 8.01 ppm (d, J_d = 8.2 Hz, 1H), 7.92 ppm (d, J_d = 8.8 Hz, 2H), 7.86 ppm (d, J_d = 8.2 Hz, 1H), 7.46 ppm (t, J_t = 7.6 Hz,1H),7.37-7.24 ppm (m, 6H), 7,19 – 7.06 ppm (m, 7H).

Methods

Fluorescence quantum yields, Φ_F, were measured by the comparative method described by Eaton and Demas [17-18], using quinine sulphate in 0.1N sulfuric acid (Φ_F = 0.55) as reference. Optical densities of sample and reference solutions were set below 0.2 at the excitation wavelength and the fluorescence spectra were corrected by using rhodamine G as reference. Sample quantum yields were evaluated by using equation (1):

$$\Phi_x = \left(\frac{Grad_x}{Grad_{Act}}\right)\left(\frac{\eta_x^2}{\eta_{Act}^2}\right)\Phi_{Act} \qquad (1)$$

where $Grad_X$ and $Grad_{Act}$ are the slope of integrated fluorescence vs. absorbance plots for the sample and the actinometer, respectively, and η_x and η_{Act} are the refractive index of sample and actinometer solutions, respectively. Geometry optimizations, energy evaluations, Franck-Condon transition calculations and Onsager cavity radius calculations were carried out with Gaussian 09W, Revision B.03 package [19].

RESULTS AND DISCUSSION

Absorption Spectra

The absorption spectrum of *DPAPBTZ* was determined in a large set of solvents of different polarity and proton donating capacity at room temperature. Figure 2 shows the absorption spectra in selected solvents representatives of the polarity scale, including non-polar, polar, and polar protic solvents. The corresponding spectral data are summarized in Table 1. *DPAPBTZ* display absorption spectra with an intense low-energy broad band with maximum wavelength near to 372 nm. The molar extinction coefficient at the maximum wavelength are high, (2.02 – 2.33) x 10^4 M^{-1} cm^{-1}. The wavelength of the absorption maximum located around of 372 nm is almost insensitive on the solvent polarity. Only in non-polar solvents, such as cyclohexane and heptane, a fair vibrational fine structure was observed, consistent with the π-π^* nature of the transition and to some extent due to the partial double bond

character of the bridge between the thiazole ring and the 4-diphenylamino phenyl substituent [20].

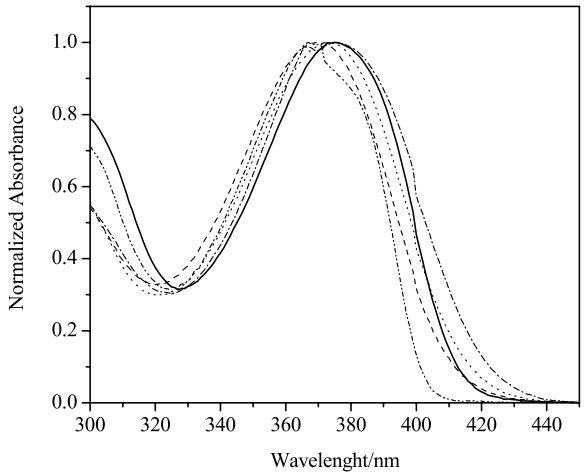

Figure 2. *Absorption spectra of DPAPBTZ in selected solvents: ── Benzene, --- ACN, ····Methanol, –·–·· Formamide, –···–·· Heptane.*

We calculated the spectra employing the DFT formalism (B3LYP-6311g+) for structure optimization and ZINDO-S, CIS and TD-SCF to calculate the vertical Franck-Condon transitions. Our calculations in gas phase, show that the CIS (6-31g basis) underestimate λ_{max} values by a large amount, whereas ZINDO-S and TD-SCF (DFT 6311+g level of theory), predict vertical transitions at 386.6 nm (*f* = 1.13) and 384.7 nm (*f* = 0.86), respectively, in good agreement with the experimental values. Inclusion of the PCM solvation model, red-shifts the low energy vertical Franck-Condon transition when methanol (395 nm) and water (406 nm) are employed as solvents. In addition, molecular orbital analysis indicates a $\pi-\pi*$ transition from valence HOMO orbital to the LUMO orbital. These results are comparable to those reported for benzothiazole-based fluorophores [3,15] and structurally related compounds such as benzoxazoles [21].

Emission Spectra

DPAPBTZ exhibits an intense emission spectrum. The position of the fluorescence maximum is strongly affected by the solvent polarity, a red-shift being observed upon increasing the solvent polarity (Figure 3). Such behavior indicates that the fluorescent state would be a highly polar state with an important charge transfer character. The relevant absorption and emission parameters in the solvent set employed are included in Table 1.

A deeper rationalization of solvent-induced shift of the fluorescence spectra can be obtained from the analysis of the fluorescence maximum dependence on microscopic solvent parameters by employing linear solvation energy relationship, LSER, equations.

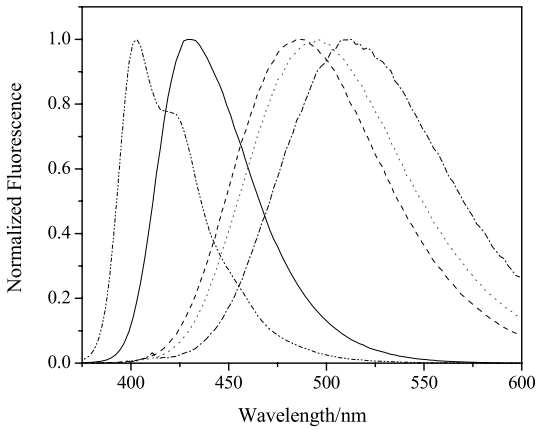

Figure 3*. Normalized fluorescence spectra of DPAPBTZ in solvents representatives of the polarity scale: ── Benzene, --- ACN, ···· Methanol, –·–·· Formamide, –···–·· Heptane.*

Table 1*.Absorption and fluorescence spectral propierties of DPAPBTZ in protic and non-protic solvents*

	Solvent	$\varepsilon/M^{-1}cm^{-1}$	λ^{abs}_{max}/nm	λ^{em}_{max}/nm	$\Delta Stokes/cm^{-1}$	Φ_F
1	Acetone	22765	372	471	5650	0.56
2	ACN	21259	370	487	6493	0.47
3	Benzene	23310	375	430	3411	1.00
4	1-Butanol		372	470	5605	0.71
5	Cyclohexane	21978	370	405	2336	1.00
6	Chloroform		376	456	4666	0.85
7	Methylene dichloride		375	466	5207	0.75
8	Dioxane	22115	373	437	3926	1.00
9	Dimethylacetamide		375	476	5658	0.60
10	DMF	23009	373	482	6063	0.54
11	DMSO	23140	375	488	6175	0.53
12	Ethanol		373	481	6020	0.56
13	Ethyl acetate		371	448	4633	0.40
14	Ethyl ether		376	430	4714	0.62
15	Formamide		373	508	6608	0.21
16	n-Heptane		373	407	4587	0.91
17	Methanol	22098	374	495	6536	0.30
18	2-Propanol		372	468	5514	0.36
19	Trifluoroethanol	20200	372	502	5514	0.01
20	Tetrahydrofuran		374	448	4416	0.77
21	Toluene		376	431	3393	0.98
22	Water		372	462	5236	0.03

To do this, we employed the semiempirical solvatochromic equation of Taft, Kamlet et al. (equation 2)[22,23]:

$$\bar{\nu}_F = \bar{\nu}_0 + a\pi^* + d\,\delta + b\alpha + c\beta + h\rho_H^2 \qquad (2)$$

In equation (2), π^* accounts for polarizabilities and dipolarities of solvent [24,25], δ is a correction term for polarizability, α corresponds to the hydrogen bond donor solvent ability, HBD, β indicates solvent capability as a hydrogen bond acceptor, HBA, and ρ_H is the Hildebrand parameter, a measure of disruption of solvent-solvent interactions in creating a cavity [22]. The coefficients of the LSER equation (equation (2)) obtained by multilinear regression analysis of the dependence of $\bar{\nu}_F$ on the solvent parameters are given in Table 2 and the correlation between the experimental and calculated values of the fluorescence maximum is shown in Figure 4. This analysis is supported by purely statistical criteria. To sum up, sample size, N, correlation coefficient, R, standard deviation, SD, and the Fisher index of equation reliability, F, indicates the quality of the overall correlation equation. The reliability of each term is indicated by t-statistic, t-stat, and the variance inflation factor, VIF. Suitable quality is indicated by large N, F, and t-stat values, small SD values, and R and VIF values close to one [26]. Also, we analyzed the dependence of the fluorescence maximum on solvent by using the solvent parameters proposed by Catalán et al., the SPP general solvent scale [27], the SA [28] and SB [29] specific solvent scales. These parameters are orthogonal and support the use of these scales for the multiparametric analysis of data sets sensitive to the solvent effect on the basis of equation 3:

$$\bar{\nu}_F = \bar{\nu}_0 + aSPP + bSA + cSB \qquad (3)$$

where SPP, SA and SB are the corresponding polarity/polarizability, acidity and basicity values for a solvent; coefficients *a*, *b* and *c* denote the sensitivity of the measured property to such effects; and $\bar{\nu}_0$ is the property value in the absence of solvent (i.e. the gas phase, which is given a zero value in these scales). Each of these scales (SPP, SB and SA) has previously been correlated with other solvent scales and found to be pure scales for the respective effects.

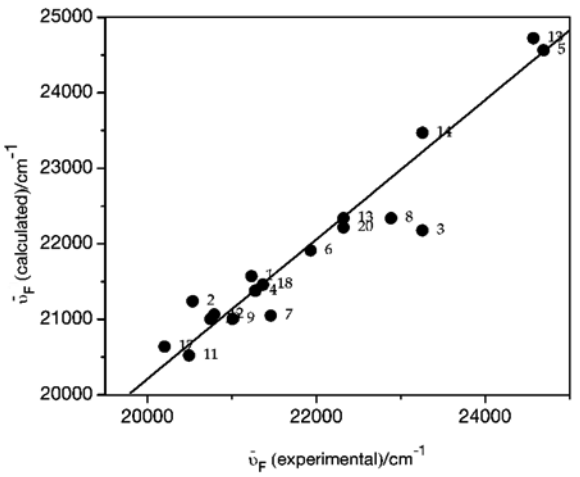

***Figure 4**. Plot of $\bar{\upsilon}^{Em}_{Max}$(calculated) vs. $\bar{\upsilon}^{Em}_{Max}$(experimental). Calculated $\bar{\upsilon}^{Em}_{Max}$ obtained according to the equation $\bar{\upsilon}$ = 24563.1-4042.2π^*-1528.6 α. Labels correspond to the list of Table 1.*

The coefficients of the SPP equation obtained by multilinear regression analysis for the dependence of the fluorescence maximum on solvent parameters are given in Table 2 and the correlation between the experimental and calculated values of the fluorescence maximum is shown in Figure 5.

Results in Table 2 show that not all descriptors are important. Descriptor coefficients accepted in the correlation equation were those that have a significance level $\geq$0.95. Accordingly, both, the β and the ρ_H parameters were not included in LSER correlation for *DPAPBTZ.* The LSER coefficients in Table 2, indicate that the energy of the fluorescent state decrease in solvents with largest capacity to stabilize charges and dipoles and in strong HBD solvents. This result support an emissive state with a strong intramolecular charge transfer character which is stabilized in solvents with high π^* values. Further stabilization of the excited state is obtained from the interactions of HBD solvents with the most negative centre of the singlet excited state. We perform the optimization of the excited state using TD-DFT formalism (B3LYP-6311g+dp) and the PCM solvation model in methanol as solvent. The result, as expected, indicates that the most negative centre of the molecule in the excited state corresponds to the oxazole ring which probably undergoes hydrogen bonding like interactions with HBD solvents.

***Table 2**. Correlation equations for the dependence of the υ_{Max}^{Em} (expressed in cm^{-1}) on the solvent parameter*

$$\bar{\upsilon}_F = \bar{\upsilon}_0 + a\,\pi^* + b\,\alpha$$

	$\bar{\upsilon}_0$	a	b
Coeff	24563.1	-4042.2	-1528.6
±	225.3	349.9	208.3
t-stat	109.0	-11.5	-7.3
P(2-tail)	<0.0001	<0.0001	<0.0001
N = 19		R = 0.96	F = 100

$$\bar{\upsilon}_F = \bar{\upsilon}_0 + a\,SPP + b\,SA$$

	$\bar{\upsilon}_0$	a	b
Coeff	29141.4	-8723.8	-1740.1
±	450.4	567.6	306.7
t-stat	64.5	-15.4	-5.8
P(2-tail)	<0.0001	<0.0001	<0.0001
N = 20		R = 0.98	F = 181.9

Similar results on the solvent effect were obtained employing equation 3. With this equation, SPP and SA were included in the correlation. Furthermore, the large values of the SPP coefficient in comparison to the SA coefficient (Table 2) emphasizes the strong charge transfer character of the excited singlet, accounting for the large red-shift of the emission observed in polar solvents.

Fluorescence quantum yields measured in a series of solvent are included in Table 2. The data show that in non-polar solvents such as benzene fluorescence quantum yields are close to 1. The smaller quantum yields, around 0.03-

0.01, were found in polar protic solvents such as water and trifluoroethanol. In polar non-protic solvents, fluorescence quantum yields take intermediary values, in the range 0.6 to 0.9. These results, suggest an important increase in the dipole moment of the relaxed S_1 excited state of the molecule during its lifetime. The ICT state favoured in polar/protic solvents is consistent with the high dipole moment that characterises this state, and decays without any appreciable energy barrier [30, 31]. This extra deactivation process decreases the fluorescent efficiency of the *DPAPBTZ* fluorescent probe in polar protic solvents.

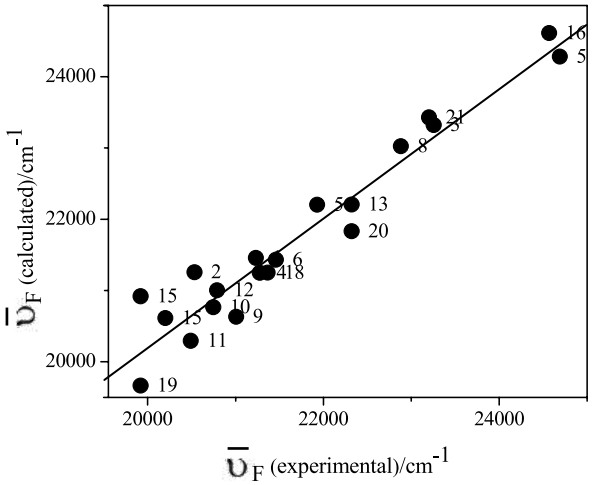

Figure 5. Plot of $\bar{\upsilon}^{Em}_{Max}$(experimental) vs. $\bar{\upsilon}^{Em}_{Max}$(calculated). Calculated $\bar{\upsilon}^{Em}_{Max}$ obtained according to the equation υ_F = 29141.4-8723.8 SPP - 1740.1 SA. Labels according the list in Table 1.

Excited State Dipolar Moment Determination

The spectral shift of the fluorescence, or more rigorously, the difference between the positions of the absorption and fluorescence maximum depends on solvent polarity function defined by dielectric constant (ε) and refractive index (*n*) of the solvent. The dipole moment change between excited- and ground states can be experimentally calculated from the Lippert–Mataga relationship, if polarizability of the solute can be neglected, i.e., a = 0 [32-33]:

$$\begin{aligned}\bar{\nu}_A - \bar{\nu}_F &= m_1 f(\varepsilon, n^2) + const. \\ &= m_1\left(\frac{\varepsilon-1}{2\varepsilon+1} - \frac{n^2-1}{2n^2+1}\right) + const.\end{aligned} \quad (4)$$

$$m_1 = \frac{(\mu_e - \mu_g)^2}{\kappa a^3} \quad (5)$$

where μ_e and μ_g are the dipole moments of the fluorophore in the excited and the ground state, respectively; *a* is a radius of the Onsager cavity, assumed to be a sphere and κ is a universal constant equal to 1.10511 x 10^{-35} C^2. A representative Lippert-Mataga plot for *DPAPBTZ* is shown in Figure 6.

Based on the calculated value of Onsager's cavity radius, 5.96 Å, and the ground-state dipole moment, 3.07 Debye, obtained from the DFT B3LYP (6311+g) optimization of the molecular geometry, the excited state dipolar moment calculated from the slopes of Lippert-Mataga plot was equal to 14.1 Debye. This value compares reasonably, within the approximations included in the calculations, with the value of 18.44 Debye obtained from the optimization of the excited singlet using the TD-SCF formalism of Gaussian 09W (DFT B3LYP (6311+g), PCM solvation model, methanol as solvent). The result indicates a significant increase of the dipolar moment in the singlet excited state as consequence of the large charge transfer taking place during the excitation of the benzothiazole derivative. The larger dipolar moment calculated for *DPAPBTZ* in the excited state reflects the donor effect of the diphenylamino group on the phenyl substituent, implying that the diphenylaminophenyl substituent in position 2 is involved in the charge-transfer process towards the oxazole acceptor center. A similar intramolecular charge transfer process has been described for analogous benzothiazole derivatives [34].

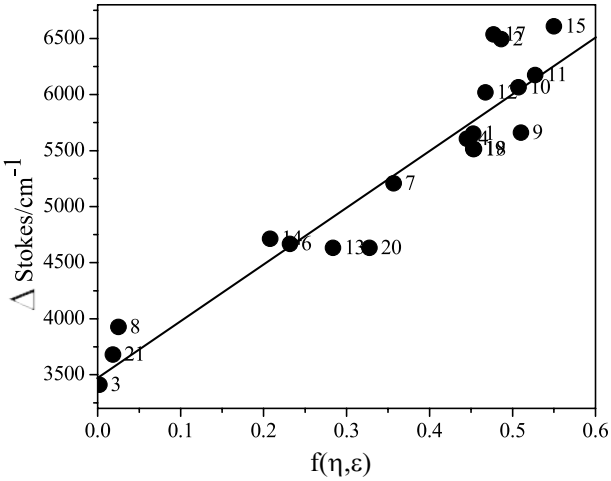

Figure 6*. Lippert–Mataga plot of the difference between absorption and fluorescence maxima on the solvent-polarity function, f(η ,ε) = (((ε –1)/(2ε + 1))–((n² –1)/(2n² + 1))) for DPAPBTZ.*

Studies in Micellar Systems

Self-association of long-chain amphiphilic molecules forms micellar aggregates in aqueous solutions, above certain concentration called critical micelle concentration, CMC. Herein, *DPAPBTZ* has been employed to determine the CMC values for the commonly used surfactants sodium dodecyl sulfate, *SDS*, triton X-100, *TX-100* and sucrose monocaprate, *SuMC*. The CMC values were calculated from the variation of the relative fluorescence intensities ($I_F/I_F(0)$) with the surfactant concentration, however the observed change in the fluorescence spectrum with the surfactant addition depends on the surfactant chemical nature. Addition of *SDS* to an aqueous solution of *DPAPBTZ* increases the fluorescence intensity and shifts the emission maxima to the red (Figure 7), whereas unexpectedly, when *TX-100* and *SuMC* are added, the fluorescence maximum is blue-shifted.

This behavior can be rationalized in terms of the *DPAPBTZ* localization in the micelle. It is obvious that the probe is not incorporated into the micelle core otherwise a noteworthy blue shift (up to aprox. 410 nm) of the emission maxima would be observed due to the non-polar nature of this microenvironment. Then the *DPAPBTZ* should be located near to the micellar interface, probably with the benzothiazole moiety towards the lipophilic tail and the diphenylamino group oriented in the direction of the interfa-

ce [35]. Consequently, red-shifting can be understood in terms of two factors, the larger stabilization of the probe ground state in water, a process markedly dominated by hydrogen bond interactions, and the greater stabilization of *DPAPBTZ* excited singlet state in the *SDS* micellar interface where the larger molecular dipole of the excited species strongly interacts with the charged interface.

The blue shift observed in *TX-100* and *SuMC* micelles can also be understood in terms of the *DPAPBTZ* localization in the interface. For sure, the transference of the probe from water media to the non-ionic, although containing hydroxyl groups, interface of *TX-100* or *SuMC* destabilize the *DPAPBTZ* ground state because hydrogen-bond interactions are broken. However, an even more important destabilization of the excited probe in the interface should take place, due to the increase of the *DPAPBTZ* dipolar moment with the excitation and the less-polar microenvironment around it as result of the presence of structured water molecules near to surfactant heads. Anyway, independently of the emission-shift, the CMC values obtained for SDS, TX-100, and SuMC, are in good agreement with those obtained by using other well-known probes [36-39].

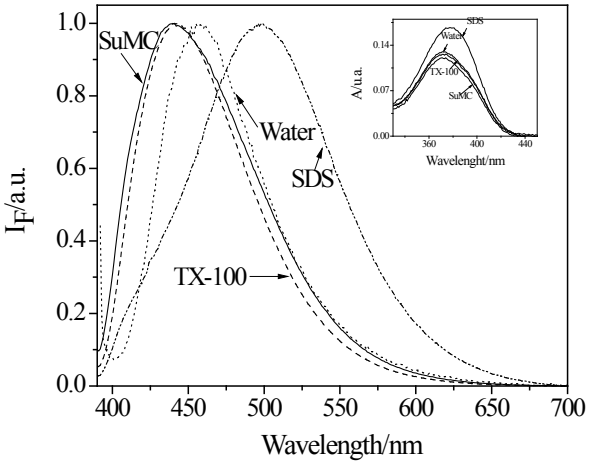

Figure 7*. Comparison of the normalized fluorescence spectra of DMAPBTZ in water and in micellar solution of various surfactants. Inset: Absorption spectra of the DPAPBTZ in the same solutions.*

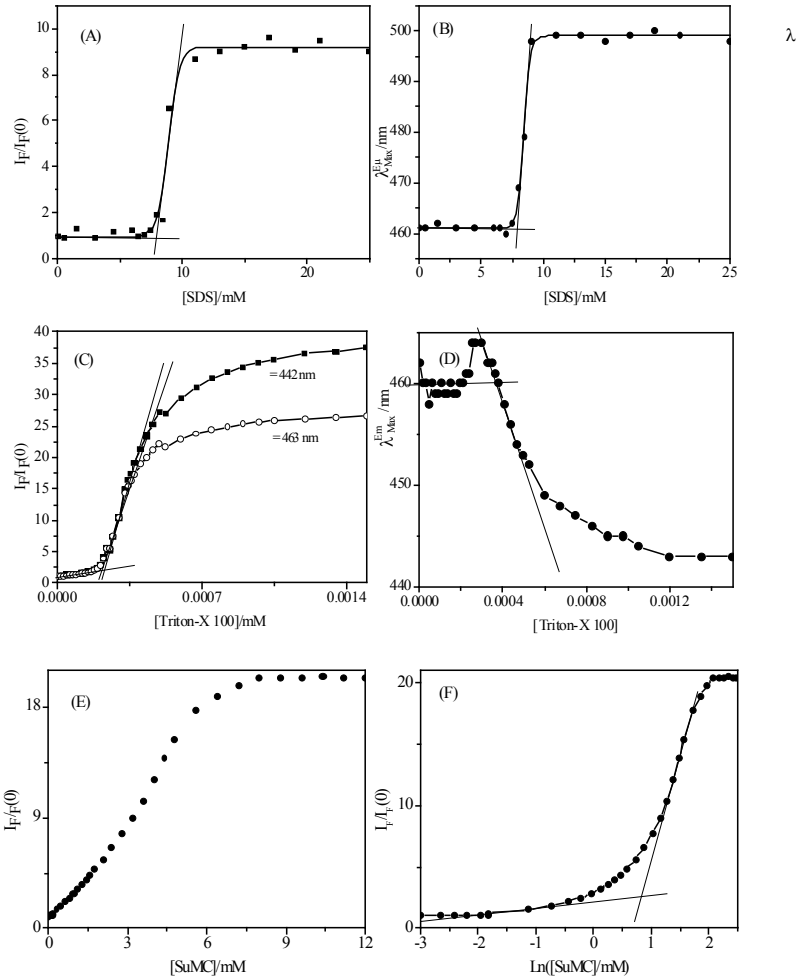

Figure 8. *(A) Dependence of the relative fluorescence intensity of DPAPBTZ measured at 498 nm on the SDS concentration, (B) Dependence of the fluorescence maxima of DPAPBTZ on the SDS concentration, (C) Dependence of the relative fluorescence intensity of DPAPBTZ measured at 463 and 442 nm on the TX-100 concentration, (D) Dependence of the fluorescence maxima of DPAPBTZ on the TX-100 concentration, (E) Dependence of the relative fluorescence intensity of DPAPBTZ measured at 442 nm on the SuMC concentration, (F) Plot of the relative fluorescence intensity of DPAPBTZ measured at 442 nm on the logarithm of SuMC mM concentration.*

Figures 8 (A) and (B) show the plots obtained for the dependence the values of $I_F/I_F(0)$ (monitored at 498 nm) and the emission maxima on the SDS concentration. From these plots CMC values of 8.0 and 7.9 mM, respectively, were obtained. When TX-100 was the surfactant, Figure 8 (C) and (D), the $I_F/I_F(0)$ values increases abruptly at the CMC, when the fluorescence intensity changes are followed at 463 nm (near to the maximum in water) or at 442 nm (the maximum in the micelle). From these plots CMC values of 0.21 and 0.22 mM were obtained. The dependence of the emission maxima on the TX-100 concentration is more complex showing an increase at low surfactant concentration (probably reflecting probe-surfactant pre-micellar interactions), and then, a slow decrease that no reflects clearly micelles formation, although a CMC value of 0.32 mM was determined, in reasonable agreement with the value obtained from the $I_F/I_F(0)$ plots. With SuMC the situation seems to be more complicated as deduced from the plot of $I_F/I_F(0)$. The fluorescence intensity increases gradually from very low SuMC concentration values, behavior that can be explained in terms of the probe interactions with the hydroxyl groups of the sucrose head of the surfactant and probably with SuMC aggregates at the pre-micellization range. In spite of this result, a CMC value for SuMC equal to 1.78 mM was be obtained from $I_F/I_F(0)$ vs. ln[SuMC] plots, in very good agreement with reported values [39].

On the other hand, we hypothesized that the dependence of the emission maxima of DPAPBTZ on the interfase nature of micelles could be used to study the incorporation of additives that modify the micelle interface. Then, we used the DPAPBTZ probe to monitor the incorporation of n-hexanol in SDS micelles.

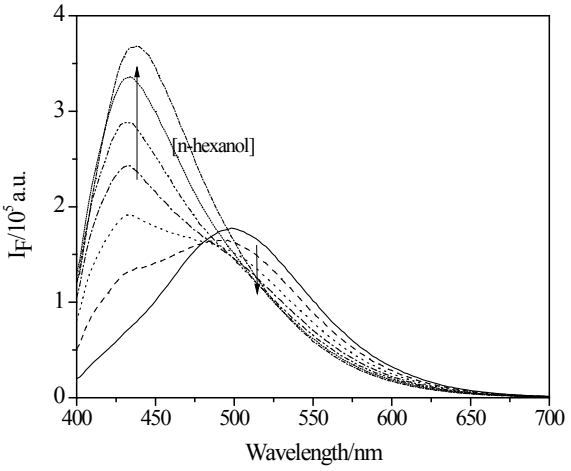

***Figure 9**. Dependence of the fluorescence spectra of DPAPBTZ in SDS micelles on the addition of n-hexanol. [n-Hexanol] = 0; 13.2; 26.4; 39.6; 52.9; 66.1; 79.3 mM.*

The addition of the alcohol to a SDS solution above the CMC results in a dramatic change of the DPAPBTZ fluorescence spectra when the concentration of DPAPBTZ is very low ([DPAPBTZ]/[SDS] < 5×10^{-4}; Figure 9). The emission maxima at 500 nm observed in SDS micelles is shifted up to 438 nm upon n-hexanol addition. This result shows that the alcohol is incorporated to the micelles modifying the nature of the interface where the probe is located. Hence, the change in the fluorescence intensity at 438 nm can be related to the partition constant of the alcohol between the micelles and the aqueous continuous pseudophase. According to Lissi et al. [40] the alcohol apparent partition constant is defined as:

$$K_A = \frac{X_A}{Y_A} \qquad (6)$$

where K_A is the apparent partition constant given in terms of mole fraction, X_A is the mole fraction of the n-hexanol in the micellar pseudophase, and Y_A is the mole fraction of the n-hexanol in the aqueous pseudophase. K_A can be calculated from a plot of the left-side of equation (7), against $C_D \times 18/(1000 - \Psi_{mic})$, using a successive approximations method:

$$\frac{(C_A)_{Tot} \times 18}{(1000 - \Psi_{mic})} = \frac{X_A}{K_A} + \frac{X_A}{(1-X_A)}\frac{C_D \times 18}{(1000 - \Psi_{mic})} \qquad (7)$$

In equation (7), $(C_A)_{Tot}$ is the total alcohol concentration. From plots $I_F/I_F(0)$ versus $(C_A)_{Tot}$ at different surfactant concentrations a set of $(C_A)_{Tot}$ values which correspond to the same $I_F/I_F(0)$ and hence with the same X_A and K_A, can be obtained. Ψ_{mic} the volume of micellar psudophase in a litre of solution was calculated using a density equal to 0.85 g/ml, independent of the composition. (C_D), the molar concentration of the micellized surfactant, was determined from the equation (8):

$$C_D = [SDS]_{Tot} - [SDS]_{free} \qquad (8)$$

where the free surfactant concentration $[SDS]_{free}$ was taken from data of Lissi et al., [40] equal to the CMC measured when the alcohol mole fraction in the aqueous pseudophase is equal to Y_A. Figure 10 shows the data plotted according to equation (7) from which K_A values as function of X_A were obtained.

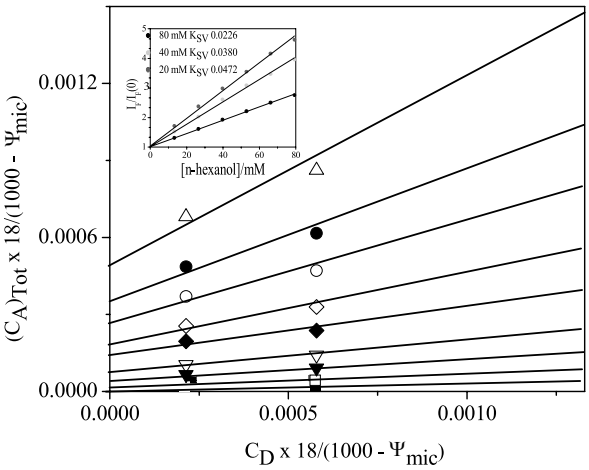

***Figure 10.** Experimental data plotted according to equation (7). $(C_A)_{Tot}$ values interpolated for $I_F/I_F(0)$ equal to: ■1.2; □1.3; ▼1.5; ▽1.7; ◆2.0; ◇ 2.3; ○2.6; ●2.7; Δ 2.8. Inset: Stern-Volmer like plots of the increase of the relative fluorescence of DPAPBTZ at 438 nm in SDS micelles as function of the n-hexanol addition.*

The values of log K_A, obtained in our experiments by measuring the increase of the DPAPBTZ fluorescence at 438

nm upon incorporation of n-hexanol to the SDS micelles is nearly constant and equal to 3.1 ± 0.09 over the X_A range between 0.18 and 0.48. This value compares reasonably well with the value of 3.3 ± 0.08 determined by Lissi el al. [40], from measurements of the pyrene fluorescence quenching by oxygen after n-hexanol addition to SDS solutions. In summary, *DPAPBTZ* shows spectroscopic and photophysical changes of the dipole moment on excitation that make this molecule a valuable fluorescent probe to determine micellar properties such as CMC and partition constants of additives included in micellar pseudophases.

ACKNOWLEDGEMENTS

Financial support from FONDECYT (grant 1080410 and 1080412) is gratefully acknowledged.

BIBLIOGRAPHY

1. S.P.G. Costa; J.A. Ferreira; G. Kirsch; A.M.F. Oliveira-Campos. J. Chem. Res.-S, 314–315, 1997.
2. J.K. Dey; S.K. Dogra. B. Chem. Soc. Jpn., 64, 3142–3152, 1991.
3. V. Hrobáriková; P. Hrobárik; P. Gajdos; I. Fitilis; M. Fakis; P. Persephonis; P. Zahradník. J. Org. Chem. 75, 3053–3068, 2010.
4. K.D. Belfield; M.V. Bondar; F.E. Hernandez; A.E. Masunov; I.A. Mikhailov; A.R. Morales; O.V. Przhonska; S. Yao. J. Phys. Chem. C, 113, 4706–4711, 2009.
5. C.C. Kitts; D.A. Vanden Bout. J. Fluoresc., 20, 881–889, 2010.
6. J.-S. Bae; S.-Y. Gwon; Y.-A. Son and S.-H. Kim. Dyes Pigments, 83, 324–327, 2009.
7. R. Sarma; B. Nath; A. Ghritlahre; J. B. Baruah. Spectrochim. Acta A, 77, 126–129, 2010.
8. R. Joseph; J.P. Chinta; C.P. Rao. Inorg. Chim. Acta, 363, 2833–2839, 2010.
9. R.M. El-Shishtawy; A.M. Asiri; S.A. Basaif; T.R. Sobahi. Spectrochim. Acta A, 75, 1605–1609, 2010.
10. V.P. Tokar; M.Y. Losytskyy; T.Y. Ohulchanskyy; D.V. Kryvorotenko; V.B. Kovalska; A.O. Balanda; I.M. Dmytruk; V.M. Prokopets; S.M. Yarmoluk; V.M. Yashchuk. J. Fluoresc., 20, 865–872, 2010.
11. J. Qi; C.-H. Tung. Bioorg. Med. Chem. Lett., 21, 320–323, 2011.
12. M. Sowmiya; A.K. Tiwari; S.K. Saha. J. Coll. Interf. Sci., 344, 97–104, 2010.
13. S.S. Jaffer; M. Sowmiya; S.K. Saha; P. Purkayastha. J. Coll. Interf. Sci., 325, 236–242, 2008.
14. A.P. Romani; A.E. da Hora Machado; N. Hioka; D. Severino; M.S. Baptista; L. Codognoto; M.R. Rodrigues; H. P. M. de Oliveira. J. Fluoresc., 19, 327–332, 2009.
15. H.-Y. Wang; G. Chen; X.-P. Xu; S.-J. Ji. Synthetic Met., 160, 1065–1072, 2010.
16. F.M. Moghaddam; G.R. Bardajee; H. Ismaili; S.M.D. Taimory. Synthetic Commun., 36, 2543-2548, 2006.
17. D.F. Eaton. Pure Appl. Chem., 60, 1107-1114, 1988.
18. J.N. Demas; G.A. Crosby. J. Phys. Chem., 75, 991-1024, 1971.
19. G.W.T. M. J. Frisch; H.B. Schlegel; G.E. Scuseria; M.A. Robb; J.R. Cheeseman; J.A. Montgomery Jr.; T. Vreven; K.N. Kudin; J.C. Burant; J.M. Millam; S.S. Iyengar; J. Tomasi; V. Barone; B. Mennucci; M. Cossi; G. Scalmani; N. Rega; G.A. Petersson; H. Nakatsuji; M. Hada; M. Ehara; K. Toyota; R. Fukuda; J. Hasegawa; M. Ishida; T. Nakajima; Y. Honda; O. Kitao; H. Nakai; M. Klene; X. Li; J.E. Knox; H.P. Hratchian; J.B. Cross; C. Adamo; J. Jaramillo; R. Gomperts; R.E. Stratmann; O. Yazyev; A.J. Austin; R. Cammi; C. Pomelli; J.W. Ochterski; P.Y. Ayala; K. Morokuma; G.A. Voth; P. Salvador; J.J. Dannenberg; V.G. Zakrzewski; S. Dapprich; A.D. Daniels; M.C. Strain; O. Farkas; D.K. Malick; A.D. Rabuck; K. Raghavachari; J.B. Foresman; J.V. Ortiz; Q. Cui; A.G. Baboul; S. Clifford; J. Cioslowski; B.B. Stefanov; G. Liu; A. Liashenko; P. Piskorz; I. Komaromi; R.L. Martin; D.J. Fox; T. Keith; M.A. Al-Laham; C.Y. Peng; A. Nanayakkara; M. Challacombe; P.M.W. Gill; B. Johnson; W. Chen; M.W. Wong; C. Gonzalez; J. A. Pople. Gaussian, Inc., Pittsburgh PA, 2003.
20. Y. Kanegae; K. Peariso; S.S. Martinez. Appl. Spectrosc., 50, 316-319(1996).
21. K. Guzow; K. Mazurkiewicz; M. Szabelski; R. Ganzynkowicz; J. Karolczak; W. Wiczk. Chem. Phys., 295, 119-130, 2003.
22. M.J. Kamlet; J.L.M. Abboud; M.H. Abraham; R.W. Taft J. Org. Chem., 48, 2877-2887, 1983.
23. A.F.M. Barton. Chem. Rev., 75, 731-753, 1975.
24. M.H. Abraham; R.M. Doherty; M.J. Kamlet; J.M. Harris; R.W. Taft. J. Chem. Soc., Perkin Trans. II, 913-920, 1987.
25. M.J. Kamlet; P. Cam; R.W. Taft; M.H. Abraham. J. Am. Chem. Soc., 103, 6060-6066, 1981.
26. D.T. Cronce; G.R. Famini; J.A. De Soto; L.Y.J. Wilson. J. Chem. Soc., Perkin Trans. II, 1293-1301, 1998.
27. J. Catalán; V. López; P. Pérez; R. Martín-Villami; J.G. Rodríguez. Liebigs Ann., 241-252, 1995.
28. J. Catalán; C. Díaz. Liebigs Ann., 1941-1949, 1997.
29. J. Catalán; C. Díaz; V. López; P. Pérez; J.L.G. de Paz; J.G. Rodríguez. Liebigs Ann., 1785-1794, 1996.
30. F. López-Arbeloa; J. Bañuelos-Prieto; V. Martínez-Martínez; T. Arbeloa-López; I. López-Arbeloa. ChemPhysChem, 5, 1762 – 1771, 2004.
31. M.F. Broglia; S.G. Bertolotti; C.M. Previtali; H.A. Montejano. J. Photoch. Photobio. A, 180, 143–149, 2006.
32. E. Lippert. Z. Naturforsch A, 6, 1962-975, 1957.
33. N. Mataga; Y. Kaifu; M. Koizumi. B. Chem. Soc. Jpn., 29, 465-470, 1956.
34. T.A. Fayed; S.S. Ali. Spectrosc. Lett., 36, 375-386, 2003.
35. T.A. Fayed, Colloid Surface A, 236, 171–177, 2004.
36. R. Chaudhuri; J. Guharay; P.K. Sengupta. J. Photoch. Photobio. A, 101, 241–244, 1996.
37. N. Sharkar; A. Datta; S. Das; K. Bhattacharyya. J. Phys. Chem., 100, 15483–15486, 1996.
38. H. Heerklotz; J. Seelig. Biophys. J., 78, 2435–2440, 2000.
39. N. Becerra; C. Toro; A. L. Zanocco; E. Lemp; G. Gunther. Colloid Surface A, 327, 134-139, 2008.
40. E. B. Abuin; E. A. Lissi. J. Colloid Interf. Sci., 95, 198–203, 1983.